Supporting Information

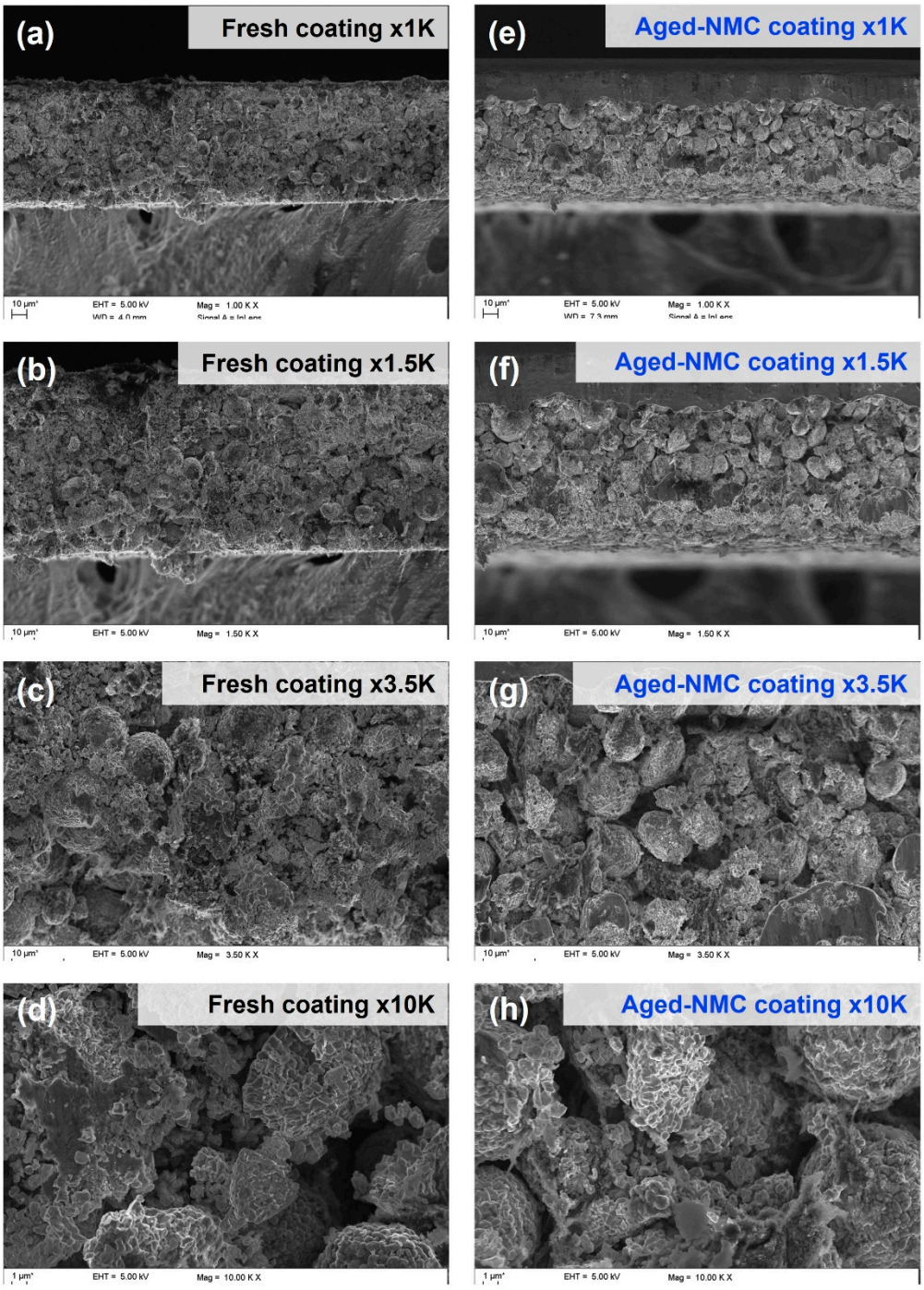

Figure S1. Cross section SEM images obtained from (a-d) Fresh and (e-f) Aged-NMC coatings at different magnifications: x1000 (a,e), x1500 (b,f), x3500 (c, g) and x10000 (d,h).

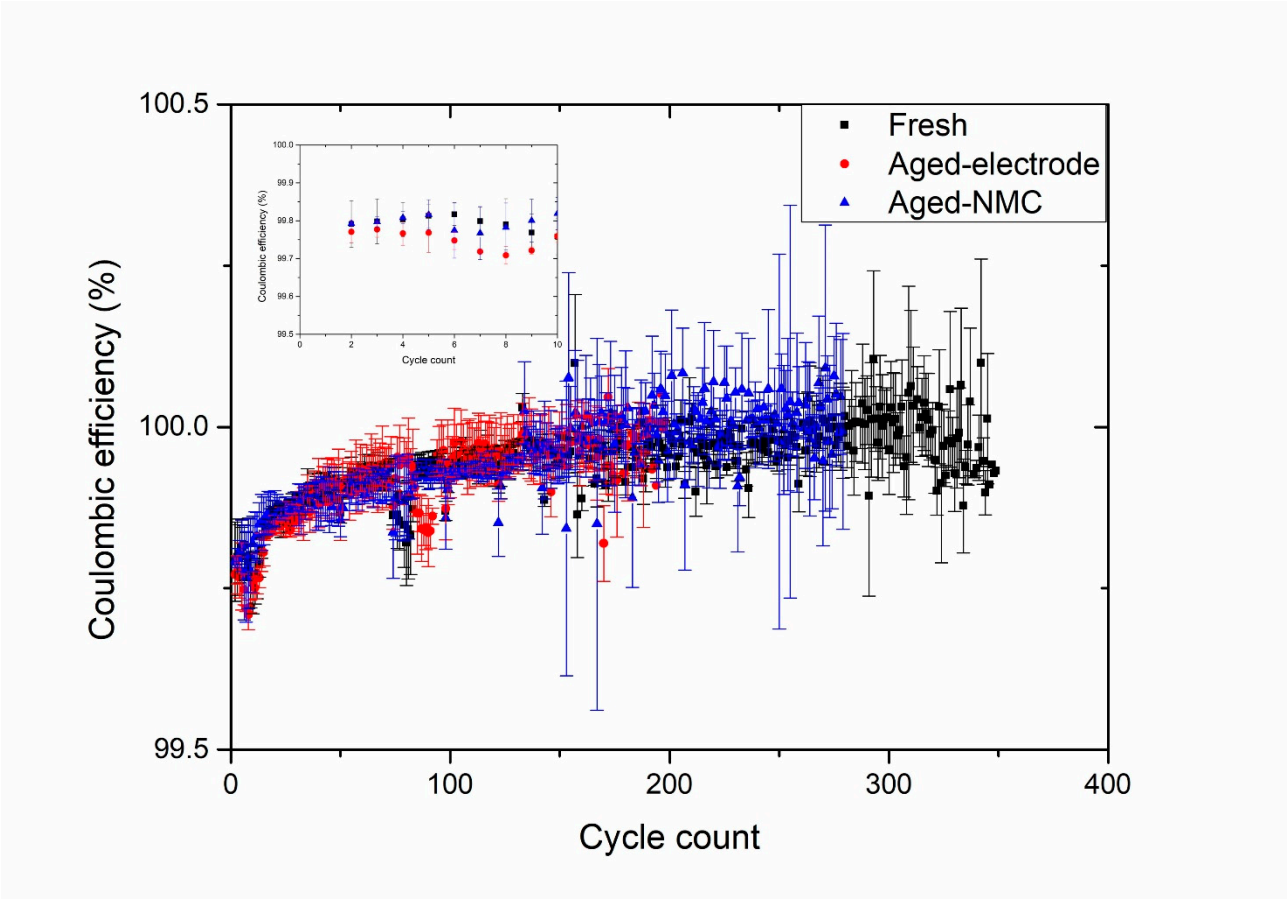

Figure S2. Coulombic efficiency values obtaining in the galvanostatic cycling experiments conducted at C/3 current rate. Zoom in of the first 10 cycles is provided in the inset figure.

Impedance spectroscopy

Bode plots collected at the beginning- (BOL) and end-of-life (EOL) of the cells analyzed are shown in Figure S3.

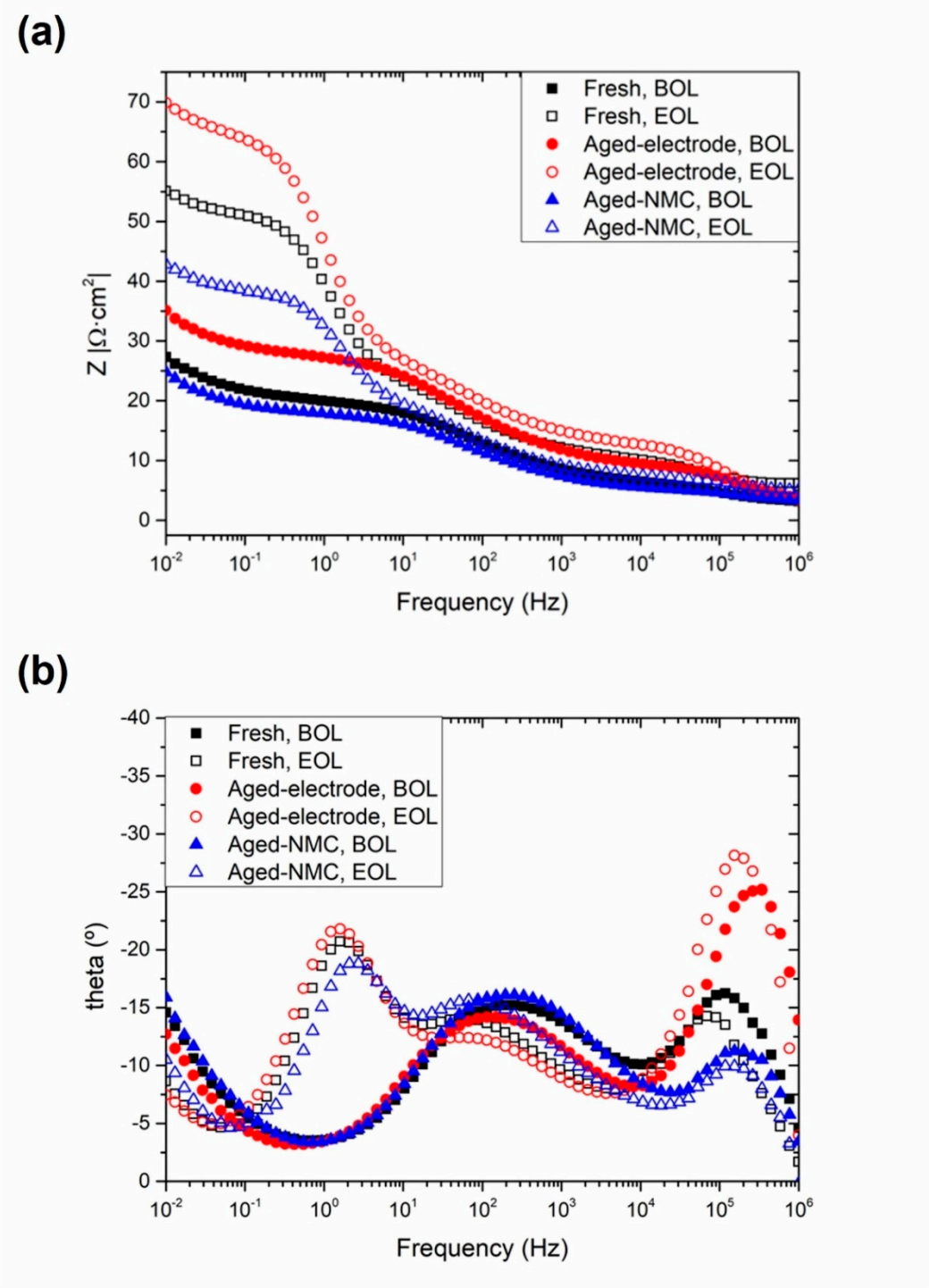

Figure S3. Bode diagrams showing (a) total impedance magnitude, Z and (b) phase angle, theta (θ), recorded at the beginning- and end-of-life of a cell.

Nyquist diagram of the cell at the BOL shows two depressed semicircles and a short tail. On the other hand, after reaching 80% SOH, the Nyquist representation of the impedance scan shows the presence of the initial two semicircles and a similar tail, but a third semicircle is also found between this tail and the second semicircle. In addition, Bode diagrams are in good agreement with the discussed Nyquist plots: there is one signal at high frequencies (~10^5 Hz) and a second one with its maximum at mid frequencies (~10^2 Hz). Furthermore, the sample at the EOL shows a third signal at low frequencies (~10^0 Hz) and the tail in the Nyquist diagram is observed by the increase of theta in the Bode diagram for both samples. Each of the semicircles was fitted using a resistance (R) in parallel with a capacitor (C) or a constant phase element (CPE). The latter simulates the contribution of an imperfect capacitor and it is used to represent porous electrodes, such as those in the current study [1]. This, the first, second and third semicircles were represented by RdlCdl, RctCPEct and Rct-2Cct-2 in the equivalent circuit [2]. The capacitance values of the first semicircles were between 10^{-5} and 10^{-7} F suggesting a double-layer charge process. On the other hand, the other two resistances were ascribed to charge transfer resistances, with capacitance values ~10^{-2} F. When analyzing the spectra in the BOL, it is likely that the charge transfer of both electrodes was merged in a single signal, while they became deconvoluted during the continuous cycling. Based on the work by Raccichini et al. [3], the contribution at higher frequencies was ascribed to the negative electrode, while that at lower frequencies was attributed to the positive electrode. In addition, the tail at the lowest frequencies and the intersection of the x-axis were fitted using a CPE [4], and a R [5], respectively. The former is associated with the diffusion of Li in the solid phase, while the latter, known in literature as the Ohmic resistance, is ascribed to the stability of the system, particularly the electrolyte, the separator, and the connections of the cell/wiring. The obtained impedance spectra were fitted with the described equivalent circuits. The results are compiled in Table S1.

Table S1. Resistance values obtained from the fitting of the impedance spectra of the cells consisting in Fresh-electrode, Aged-NMC and Aged-electrode cathodes and graphite anodes at the beginning (BOL) and end of life (EOL).

Sample	**Rohm/Ω·cm²**	**Rdl/Ω·cm²**	**Rct/Ω·cm²**	**Rct-2/Ω·cm²**
Fresh electrode BOL	3.14 ± 0.32	2.39 ± 0.14	0.27 ± 0.10	
Fresh electrode EOL	4.68 ± 1.50	3.04 ± 0.28	25.96 ± 5.26	18.77 ± 2.21
Aged-NMC BOL	2.98 ± 0.95	1.45 ± 0.84	0.13 ± 0.08	
Aged-NMC EOL	4.75 ± 1.00	1.73 ± 0.28	17.25 ± 2.25	21.00 ± 7.83
Aged-electrode BOL	3.18 ± 0.12	5.29 ± 0.31	0.24 ± 0.01	
Aged-electrode EOL	3.95 ± 0.29	6.82 ± 0.38	30.57 ± 8.28	25.16 ± 3.32

DVA of the cells

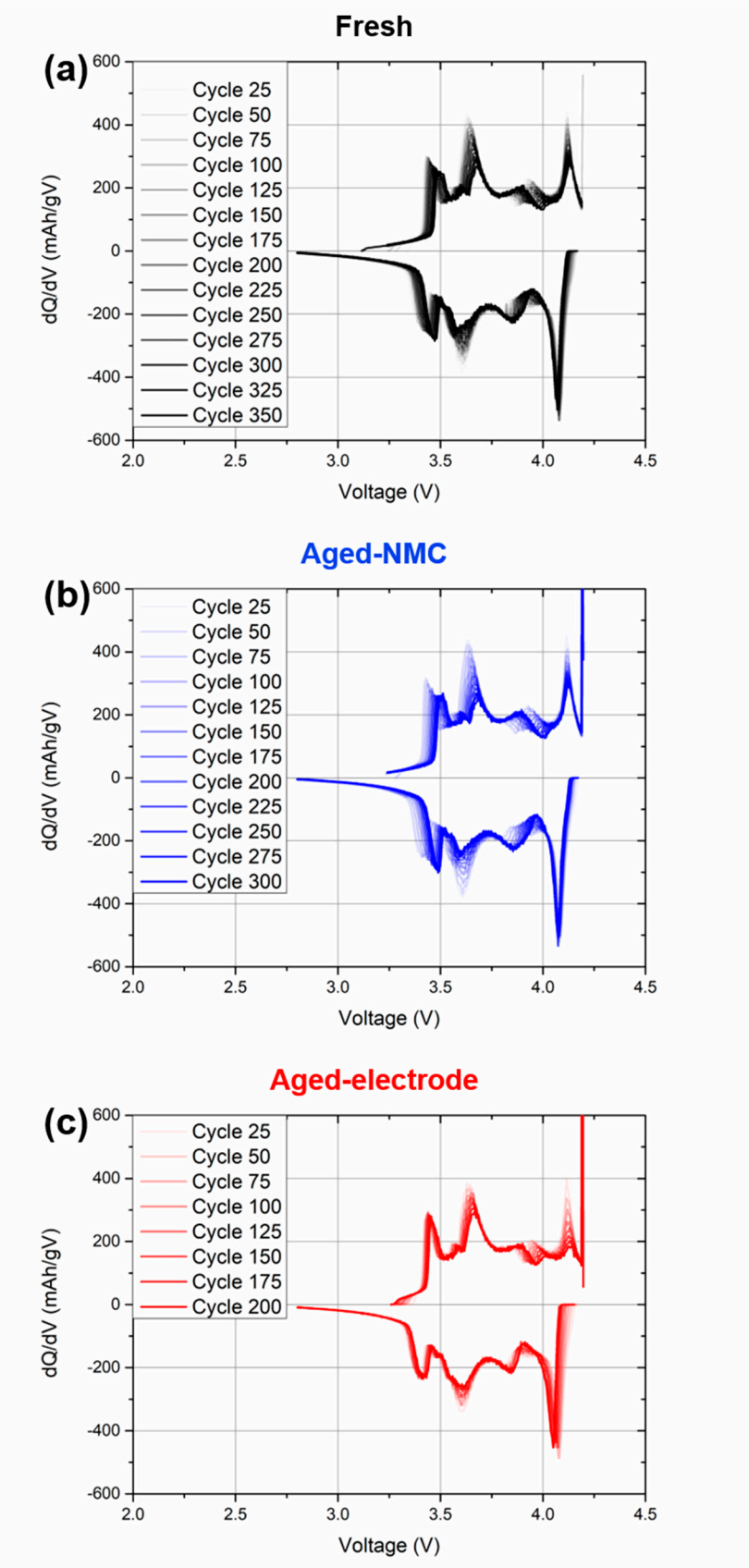

Figure S4. DVA of the cells with the (a) Fresh, (b) Aged-NMC and (c) Aged-electrode cathodes during all their cycle life.

Materials characterization

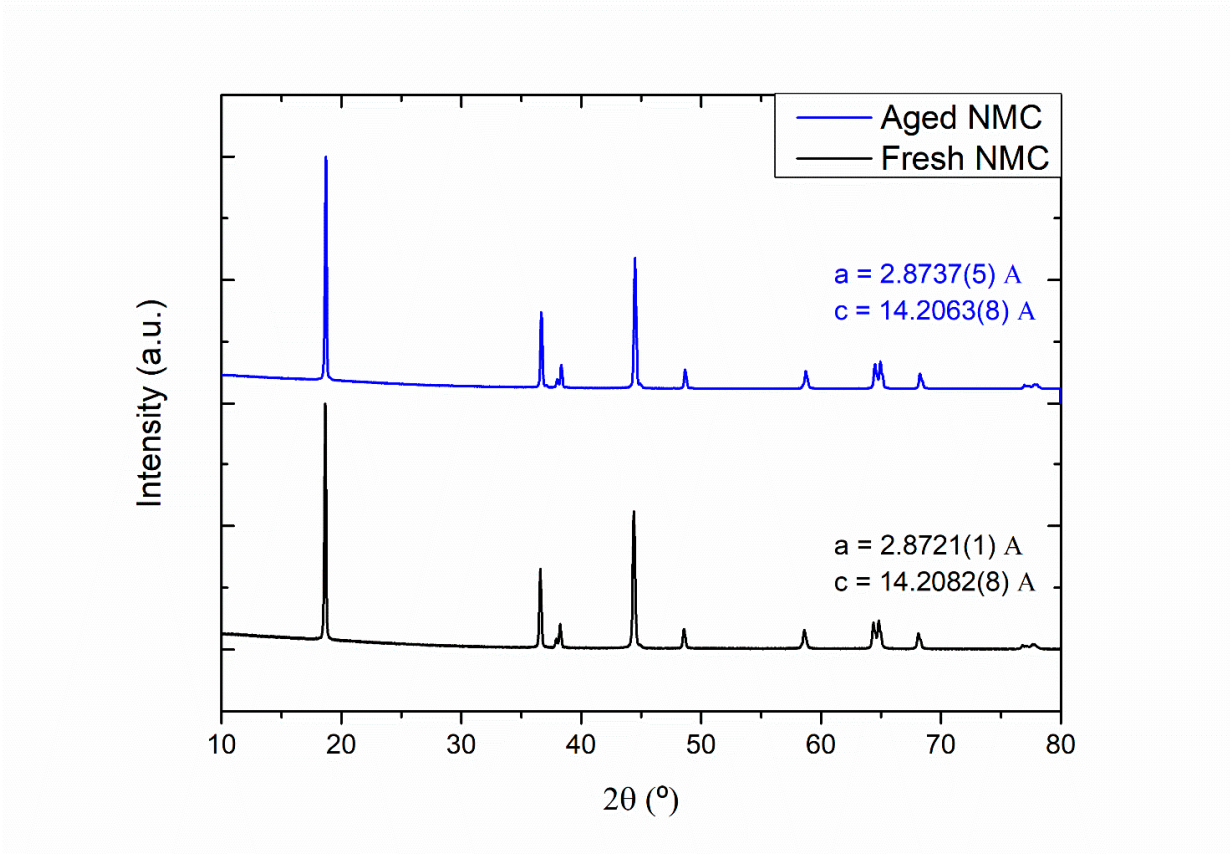

Figure S5. XRD patterns of the fresh (black line) and aged (blue line) NMC powders.

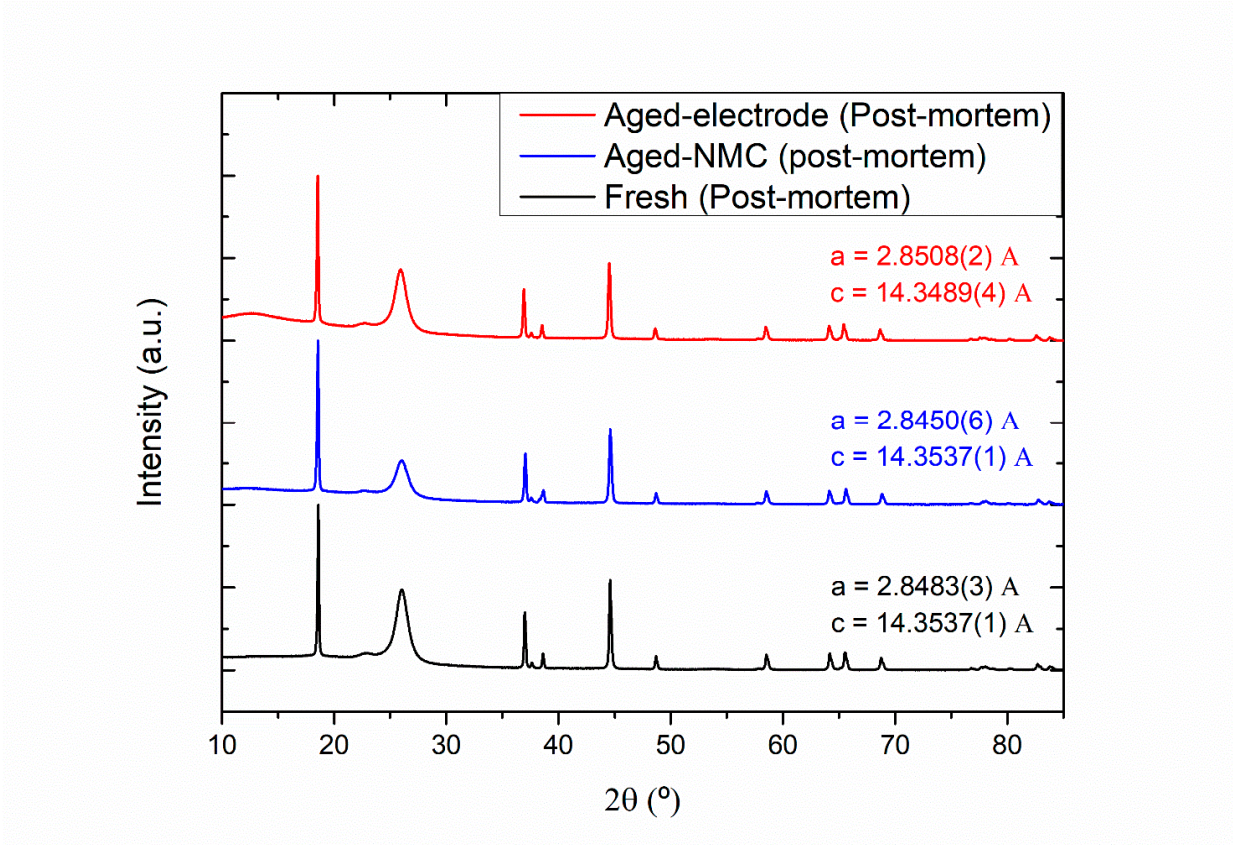

Figure S6. XRD patterns of the post-mortem Fresh (black line) and Aged-NMC (blue line) and Aged-electrode cathodes.

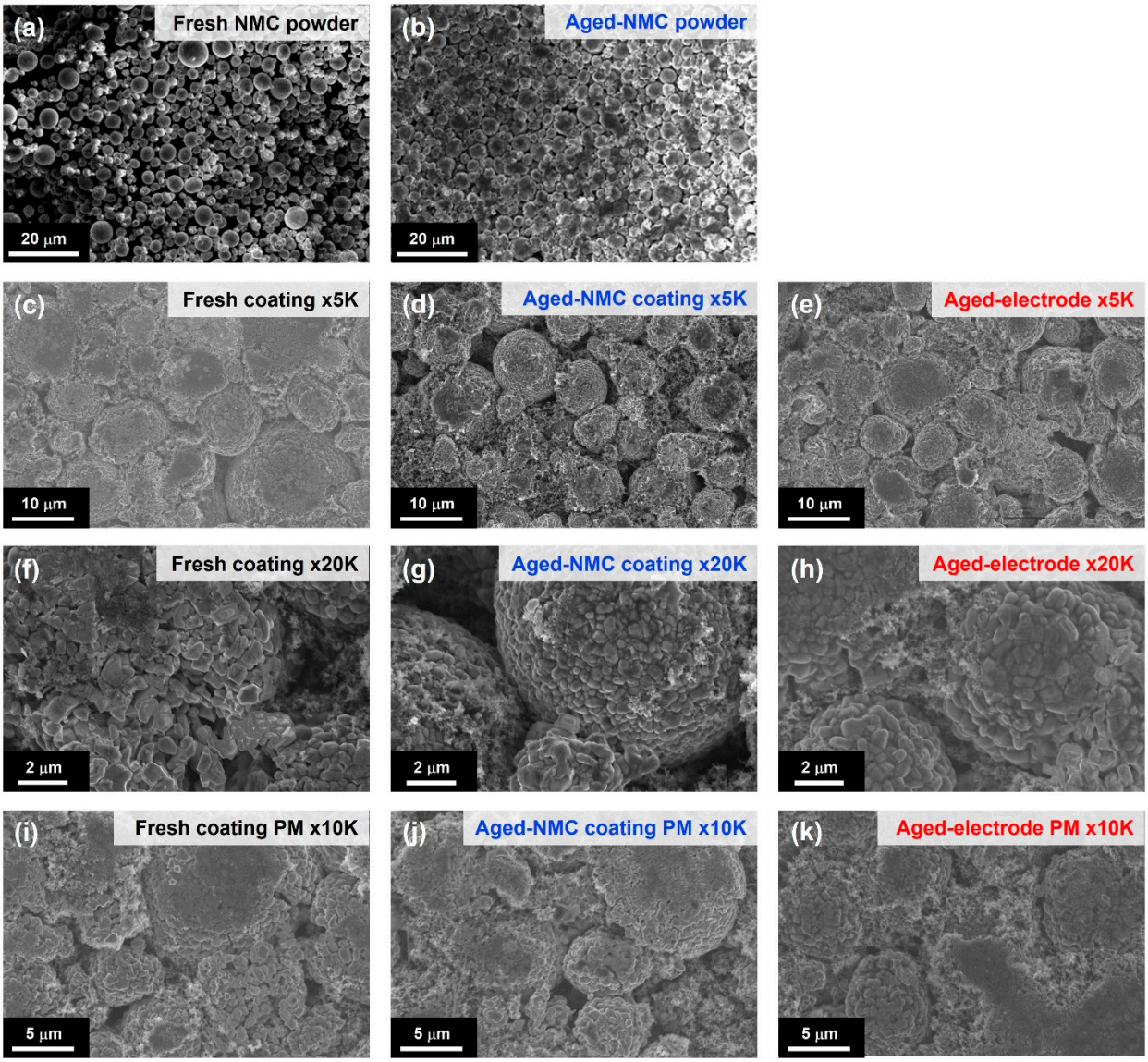

Figure S7. SEM images obtained from (a) fresh and (b) aged NMC powder. Micrographs at 5K magnification of (c) Fresh, (d) Aged-NMC and (e) Aged-electrode coatings. Micrographs at 20K magnification of (f) fresh, (g) Aged-NMC and (h) Aged-electrode coatings. Micrographs at 10K magnification of (i) Fresh, (j) Aged-NMC and (k) Aged-electrode post-mortem (PM) electrodes.

Table S2. Signals from the XPS spectra of the fresh and aged NMC powder and results from the fittings, beam energy (BE) of these signals, full width at half maximum (FWHM) of the fittings, area calculates from the fittings and atomic percentage calculated from this area.

	Fresh NMC					Aged NMC			
Signal	**Peak BE / eV**	**FWHM / eV**	**Area / CPS.eV**	**Atomic %**	**Signal**	**Peak BE / eV**	**FWHM / eV**	**Area / CPS.eV**	**Atomic %**
C1s A	284.9	1.69	16026.5	11.77	C1s A	284.97	1.83	15695.46	15.09
C1s B	286.33	2.19	6803.25	5.00	C1s B	286.4	2.87	5984.87	5.76
C1s C	289.39	2.08	4535.79	3.34	C1s C	289.83	1.91	8522.16	8.20
O1s A	529.16	1.6	14026.7	3.74	O1s A	529.33	1.71	19120.05	6.67
O1s B	531.71	2.53	124980.72	33.31	O1s B	531.73	2.32	110348.44	38.51
Li1s A	55.05	2.09	1062.85	12.48	Li1s A	54.99	2.03	1325.37	20.37
Co2p1	795.18	2.59	1786.92	0.24	Co2p1	795.47	2.65	2780.57	0.49
Mn2p1	653.91	2.3	2270.38	0.43	Mn2p1	653.93	3.02	3415.88	0.85
Ni2p	854.99	3.27	42850.82	1.77	Ni2p	855.17	3.4	74500.1	4.05

Table S3. Signals from the XPS spectra of the Fresh and Aged-NMC and Aged-electrode coatings before electrochemical tests and results from the fittings, beam energy (BE) of these signals, full width at half maximum (FWHM) of the fittings, area calculates from the fittings and atomic percentage calculated from this area.

	Fresh				Aged-NMC				Aged-electrode			
Signal	**Peak BE / eV**	**FWHM / eV**	**Area / CPS.eV**	**Atomic %**	**Peak BE / eV**	**FWHM / eV**	**Area / CPS.eV**	**Atomic %**	**Peak BE / eV**	**FWHM / eV**	**Area / CPS.eV**	**Atomic %**
C1s A	284.32	1.15	39055.25	15.63	284.46	1.27	31419.76	12.55	284.3	1.14	22676.8	8.19
C1s B	285.6	2.49	63917.34	25.58	285.58	2.46	82600.46	33.01	285.65	2.46	64168.89	23.17
C1s C	288.93	2.96	12504.01	5.01	288.65	2.54	9953.83	3.98	289.17	2.61	12801.88	4.63
C1s D	290.39	1.74	25522.64	10.22	290.67	1.96	23755.47	9.5	290.39	1.81	29706.44	10.73
O1s A	531.45	1.66	40281.33	5.85	531.61	1.94	57418.63	8.33	531.52	1.99	103877.06	13.61
O1s B	532.29	2.86	29394.09	4.27	532.97	2.19	16954.29	2.46	532.97	2.19	16954.29	2.22
O1s C	534.53	1.53	2608.21	0.38					533.18	2	13498.68	1.77
F1s A	687.48	1.88	161618.79	17.16	687.88	2.09	167448.7	17.75	687.47	1.92	183448.83	17.57
F1s B	688.36	2.09	73020.04	7.75	689.04	2.27	31968.99	3.39	688.39	2.07	84210.28	8.07
F1s C	688.7	1.82	3108.17	0.33	688.7	1.82	3108.17	0.33	688.7	1.82	3108.17	0.3
Li1s A	54.97	1.75	1220.99	7.81	55.11	1.93	1360.92	8.69	54.93	1.77	1563.93	9.03
Mn2p1									654.31	0	150.15	0.01
Ni2p									855.31	3.22	30176.06	0.62
Co2p1									795.68	0.32	1201.07	0.08

Table S4. Signals from the XPS spectra of the Fresh and Aged-NMC and Aged-electrode electrodes obtained from disassembled cells after electrochemical tests and results from the fittings, beam energy (BE) of these signals, full width at half maximum (FWHM) of the fittings, area calculates from the fittings and atomic percentage calculated from this area.

	Fresh				Aged-NMC				Aged-electrode			
Signal	**Peak BE / eV**	**FWHM / eV**	**Area / CPS.eV**	**Atomic %**	**Peak BE / eV**	**FWHM / eV**	**Area / CPS.eV**	**Atomic %**	**Peak BE / eV**	**FWHM / eV**	**Area / CPS.eV**	**Atomic %**
C1s A	284.58	1.46	29883	10.98	284.53	1.4	48263	16.34	284.62	1.49	31058	10.57
C1s B	285.88	1.49	26760	9.84	285.6	1.16	18464	6.25	285.78	1.31	26463	9
C1s C	287	1.6	15026	5.52	286.38	1.53	22144	7.5	286.65	1.64	20898	7.11
C1s D	288.55	2.05	9622	3.54	287.56	2.05	13296	4.5	288	1.98	9232	3.14
C1s E	290.42	1.98	23038	8.47	290.06	2.45	24789	8.4	290.29	2.06	29571	10.07
O1s A	531.59	2.25	78658	10.49	531.41	1.96	66974	8.23	531.48	2.03	64273	7.94
O1s B	533.43	2.81	62404	8.33	532.88	3.11	77678	9.55	533.25	2.91	63985	7.9
F1s A	684.97	2.13	78621	7.66	685.04	2.17	61538	5.52	685.02	2.01	64281	5.8
F1s B	687.37	2.12	142285	13.87	687.61	2.51	160366	14.4	687.57	2.33	214337	19.34
F1s C	688.38	2.18	53434	5.21	688.38	2.18	53434	4.8	688.38	2.18	53434	4.82
Li1s A	55.51	2.37	2604	15.3	55.41	2.53	2550	13.8	55.45	2.44	2559	13.92
Mn2p1	654.14	0.11	670	0.06	654.39	0.22	452	0.04	652.64	0.04	112	0.01
Ni2p	855.67	4.23	30660	0.64	855.95	4.01	32834	0.63	855.81	4.29	17262	0.33
Co2p1	795.87	0.35	1272	0.09	795.92	0.23	721	0.04	796.34	0.1	777	0.05
Co3p	59.78	1.65	743		57.2	0.79	322		59.59	3	1757	

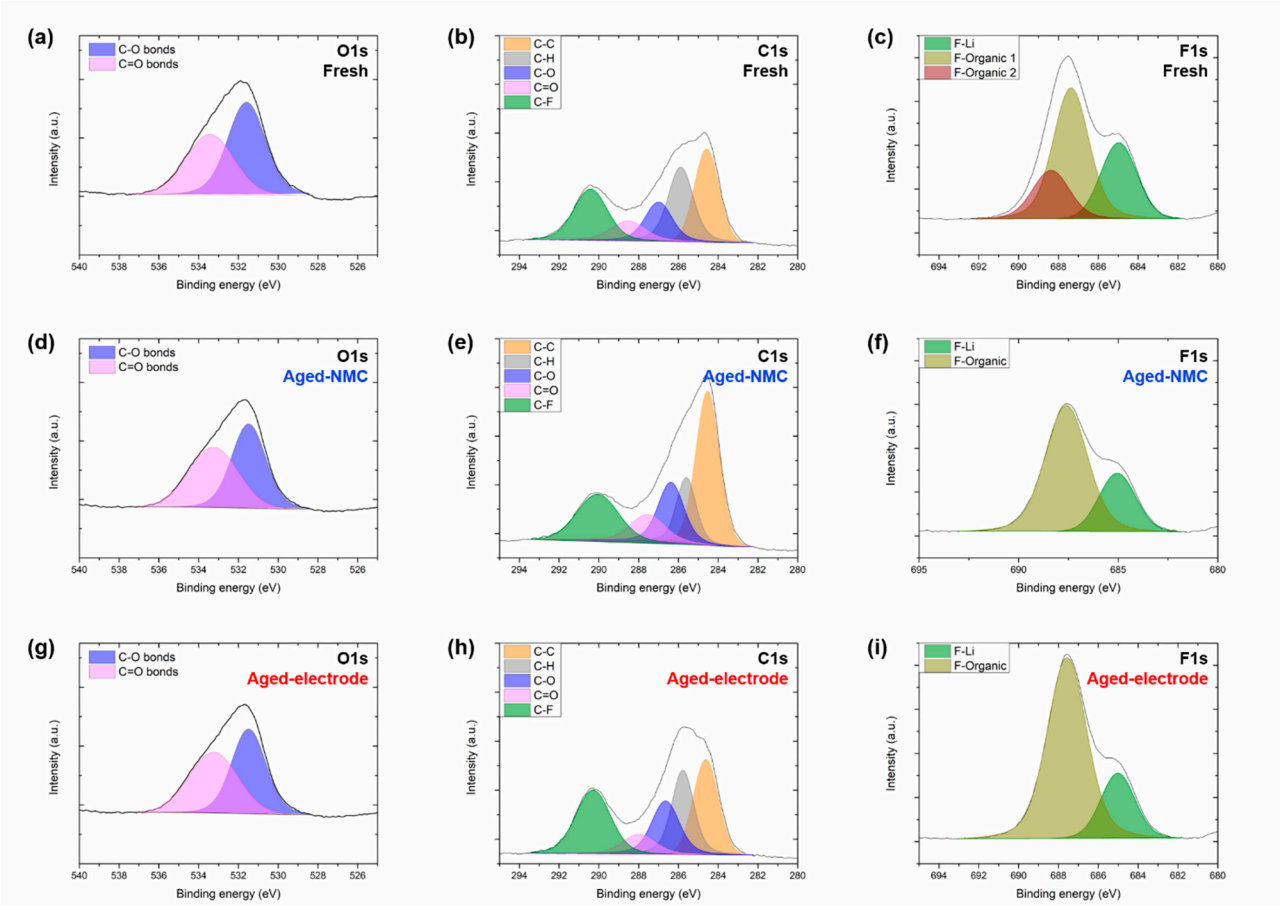

Figure S8. XPS spectra of the post-mortem electrodes. (a) O1s, (b) C1s, and (c) F1s regions of the post-mortem Fresh cathodes. (d) O1s, (e) C1s, and (f) F1s regions of the post-mortem Aged-NMC cathodes. (g) O1s, (h) C1s, and (i) F1s regions of the post-mortem Aged-electrode cathodes.

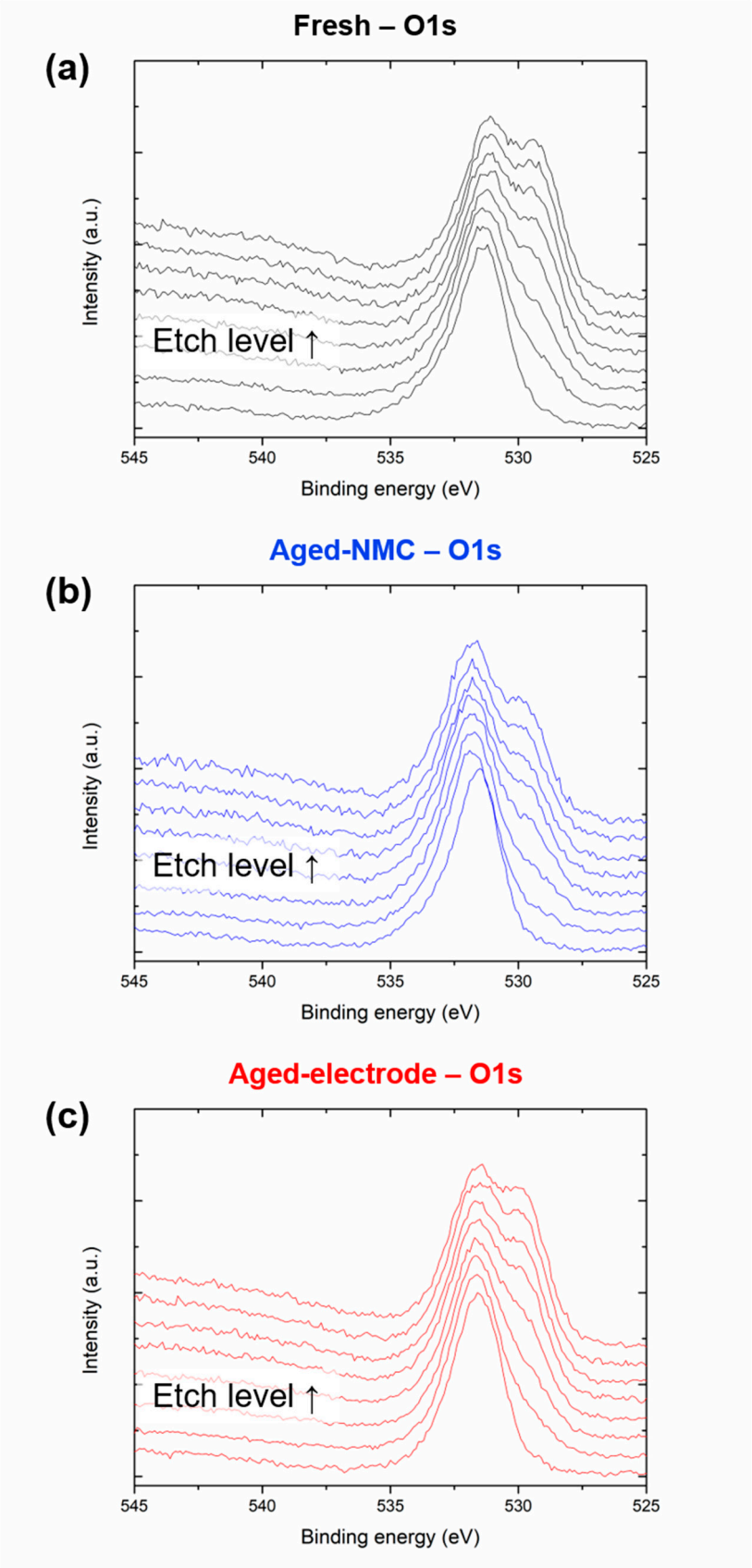

Figure S9. Depth profile XPS spectra of the different coatings. O1s regions of the (a) Fresh, (b) Aged-NMC and (c) Aged-electrode coatings.

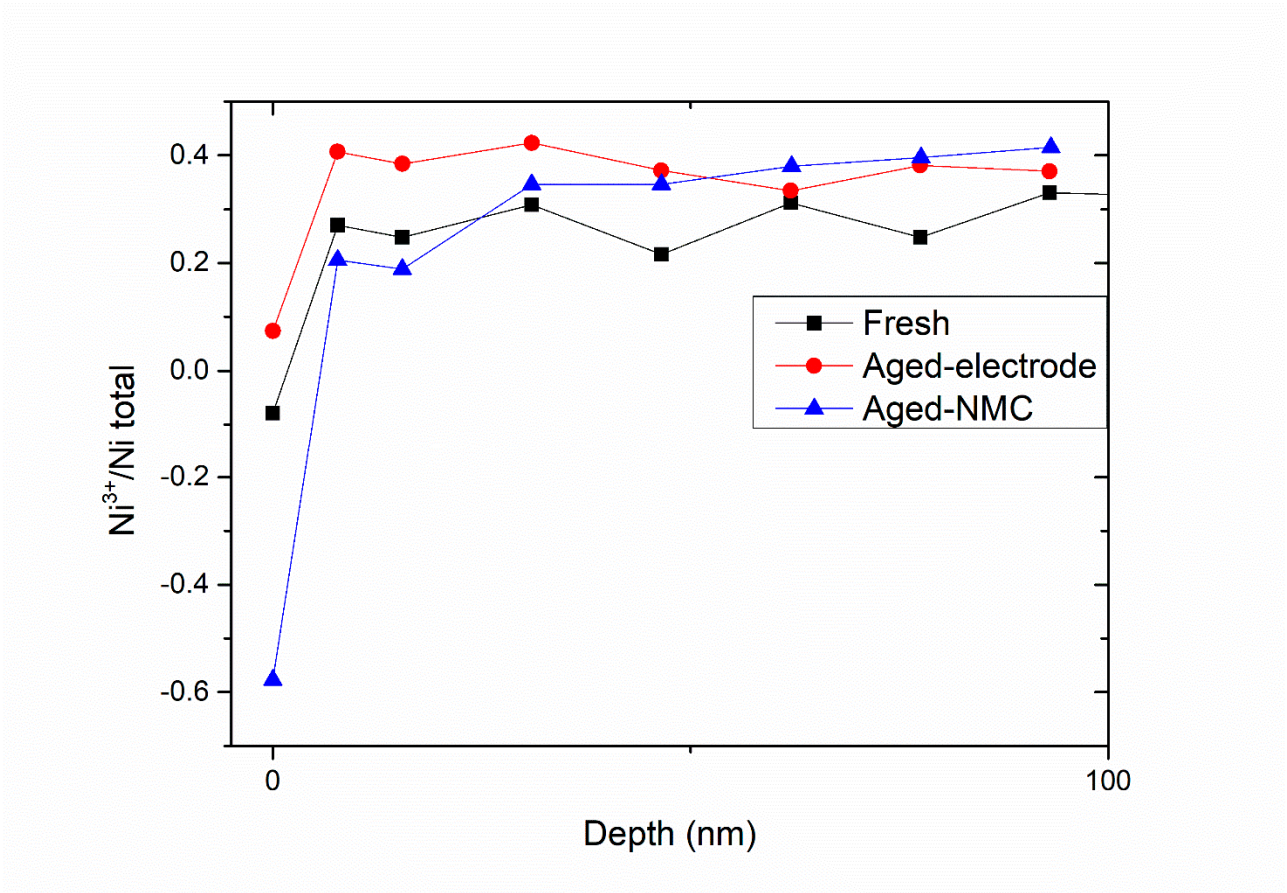

Figure S10. Ni^{3+}/Ni total fraction with the depth of the sample obtained by the methodology described in reference [6] for the Fresh (black squares), Aged-electrode (red circles) and Aged-NMC (blue triangles) coatings.

References

1. Landa-Medrano, I.; Eguia-Barrio, A.; Sananes-Israel, S.; Lijó-Pando, S.; Boyano, I.; Alcaide, F.; Urdampilleta, I.; De Meatza, I. In Situ Analysis of NMC | graphite Li-Ion Batteries by Means of Complementary Electrochemical Methods. *J. Electrochem. Soc.* **2020**, *167*, 090528. https://doi.org/10.1149/1945-7111/ab8b99.
2. Li, X.; Colclasure, A.M.; Finegan, D.P.; Ren, D.; Shi, Y.; Feng, X.; Cao, L.; Yang, Y.; Smith, K. Degradation mechanisms of high capacity 18650 cells containing Si-graphite anode and nickel-rich NMC cathode. *Electrochim. Acta* **2019**, *297*, 1109–1120.
3. Raccichini, R.; Amores, M.; Hinds, G. Critical review of the use of reference electrodes in Li-ion batteries: A diagnostic perspective. *Batteries* **2019**, *5*, 12.
4. Le, H.T.; Kalubarme, R.S.; Ngo, D.T.; Jang, S.Y.; Jung, K.N.; Shin, K.H.; Park, C.J. Citrate gel synthesis of aluminum-doped lithium lanthanum titanate solid electrolyte for application in organic-type lithium–oxygen batteries. *J. Power Sources* **2015**, *274*, 1188–1199.
5. Huang, L.H.; Chen, D.; Li, C.C.; Chang, Y.L.; Lee, J.T. Dispersion homogeneity and electrochemical performance of Si anodes with the addition of various water-based binders. *J. Electrochem. Soc.* **2018**, *165*, A2239–A2246.
6. Bondarchuk, O.; LaGrow, A.P.; Kvasha, A.; Thieu, T.; Ayerbe, E.; Urdampilleta, I. On the X-ray photoelectron spectroscopy analysis of LiNixMnyCozO2 material and electrodes. *Appl. Surf. Sci.* **2021**, *535*, 147699. https://doi.org/10.1016/j.apsusc.2020.147699.